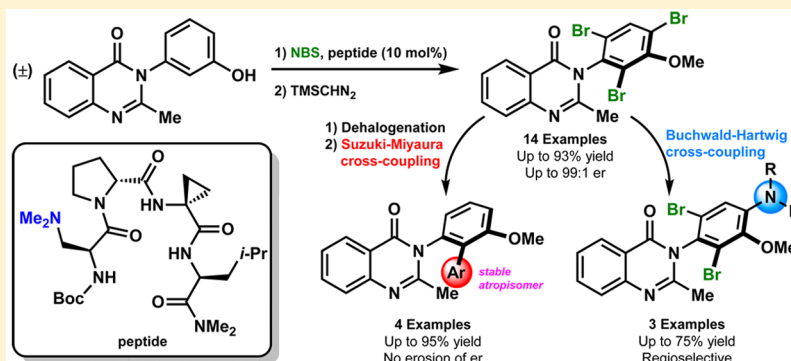


# Enantioselective Synthesis of 3-Arylquinazolin-4(3*H*)-ones via Peptide-Catalyzed Atroposelective Bromination

Matthew E. Diener,<sup>†</sup> Anthony J. Metrano,<sup>†</sup> Shuhei Kusano,<sup>‡</sup> and Scott J. Miller\*<sup>‡</sup>

Department of Chemistry, Yale University, New Haven, Connecticut 06520-8107, United States

**S** Supporting Information



**ABSTRACT:** We report the development of a tertiary amine-containing  $\beta$ -turn peptide that catalyzes the atroposelective bromination of pharmaceutically relevant 3-arylquinazolin-4(3*H*)-ones (quinazolinones) with high levels of enantioinduction over a broad substrate scope. The structure of the free catalyst and the peptide–substrate complex were explored using X-ray crystallography and 2D-NOESY experiments. Quinazolinone rotational barriers about the chiral anilide axis were also studied using density functional theory calculations and are discussed in light of the high enantioselectivities observed. Mechanistic studies also suggest that the initial bromination event is stereodetermining, and the major monobromide intermediate is an atropisomerically stable, mono-*ortho*-substituted isomer. The observation of stereoisomerically stable monobromides stimulated the conversion of the tribromide products to other atropisomerically defined products of interest. For example, (1) a dehalogenation Suzuki–Miyaura cross-coupling sequence delivers *ortho*-arylated derivatives, and (2) a regioselective Buchwald–Hartwig amination procedure installs *para*-amine functionality. Stereochemical information was retained during these subsequent transformations.

## INTRODUCTION

It is now becoming well-appreciated that atropisomerism<sup>1</sup> is an issue of significant importance in medicinal chemistry.<sup>2</sup> Chiral compounds that exist as separate atropisomers may present advantages if they have sufficiently low barriers to racemization, such that dynamic kinetic resolution<sup>3</sup> is possible during selective binding to a targeted biological receptor. However, if the opposite atropisomer binds to an off-target receptor, alternative, and even deleterious, effects may ensue.<sup>4</sup> Perhaps these scenarios are behind an increasing number of reports,<sup>5</sup> and even patents,<sup>6</sup> that describe the differential biological functions of individual atropisomers. Accordingly, synthetic efforts to prepare individual atropisomers comprise an area of significant innovation in chemistry.<sup>7</sup> Among scaffolds that present these stereochemical issues, 3-arylquinazolin-4(3*H*)-ones<sup>8</sup> (1) are an important class of compounds, whose exploding list of characterized biological properties enumerates a large swath of biochemical functions (Figure 1a).<sup>9</sup> We report herein our recent studies culminating in catalyst-dependent syntheses of atropisomeric quinazolinone bromides (2) with high levels of enantioinduction. These findings enable efficient access to a range of substituted

quinazolinones available through an atroposelective tribromination reaction, followed by either dehalogenation–cross-coupling sequences or regioselective amination reactions.

We recently demonstrated that peptide-based catalysts are effective for the atroposelective bromination of both biaryl<sup>10</sup> and tertiary benzamide scaffolds.<sup>11</sup> Gratifyingly, a related approach has also been recently reported to access chiral isoquinoline *N*-oxides using a cinchona alkaloid-derived urea catalyst.<sup>12</sup> It is interesting to note that the enantioselective synthesis of axially chiral quinazolinones is a subject with limited literature,<sup>13</sup> and most methods have involved either racemic synthesis followed by resolution or diastereoselective synthesis using chiral auxiliaries. Given the growing interest in these compounds in medicinal chemistry, we targeted a catalytic asymmetric approach (Figure 1b). Notably, unlike many biaryl compounds and benzamides, an opportunity also existed for selective preparation of atropisomerically stable mono-*ortho*-substituted quinazolinones (e.g., 3, Figure 1b), given their established high barriers to enantiome-

Received: July 28, 2015

Published: September 6, 2015

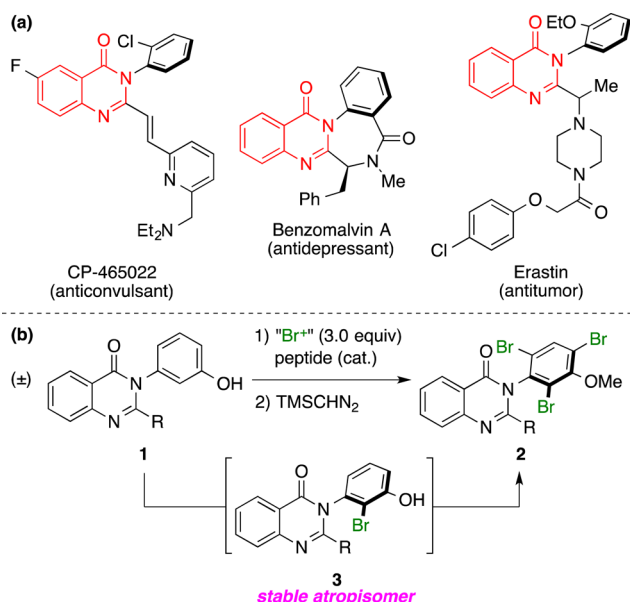


**Figure 1.** (a) Some 3-arylquinazolin-4(3*H*)-one-based bioactive compounds.<sup>9</sup> (b) Our strategy for the peptide-catalyzed atroposelective bromination of quinazolinones **1** to access enantioenriched bromides **2**.

zation.<sup>14</sup> At the same time, these issues could present fundamental challenges to the development of catalysts that might mediate dynamic kinetic resolutions.<sup>3</sup> Our assessment of these concepts is presented below.

## RESULTS AND DISCUSSION

**Catalyst Identification.** Our exploration of this intriguing system began with a study of peptide-based catalysts for the bromination of quinazolinone **1a** using the conditions described in eq 1.<sup>15</sup> Our design principle was guided by previous reports from our group, wherein we were able to embed a tertiary-amine-containing  $\beta$ -dimethylaminoalanine (Dmaa) residue within a peptide sequence that was expected to adopt a well-defined  $\beta$ -turn geometry.<sup>16</sup> In that way, we hoped to capitalize on an interaction (e.g., hydrogen bonding or even proton transfer) between the phenol of **1a** and the tertiary amine moiety of the Dmaa residue, with the potential for additional interactions provided by the functionality and chirality of the peptide (i.e., catalysts such as **4**).<sup>11</sup> Accordingly, dynamic kinetic resolution would be possible via selective docking and functionalization of one atropisomer of ( $\pm$ )-**1a** over the other.

In the absence of any catalyst, bromination of **1a** was sluggish and nonselective under the conditions we examined.<sup>17</sup> However, using triethylamine (10 mol %) as a catalyst, bromination of **1a** proceeded smoothly, providing 88% yield of racemic tribromide **2a**. Thus, we began to assess peptide-based catalysts (**4**) for this transformation, and the results of our optimization are summarized in Figure 2.<sup>18</sup> We were pleased to discover that peptide **4a**, an archetypal  $\beta$ -turn-promoting sequence that we have utilized in the past,<sup>11,19</sup> provided tribromide **2a** in 66:34 er, setting the stage for further optimization. In a number of previous instances, we have observed a marked effect of the C-terminal protecting group on the enantioselectivity of peptide-catalyzed reactions.<sup>16</sup> Comparing peptides **4a–f**, it is clear that the dimethylamide end-cap provides an advantage over the

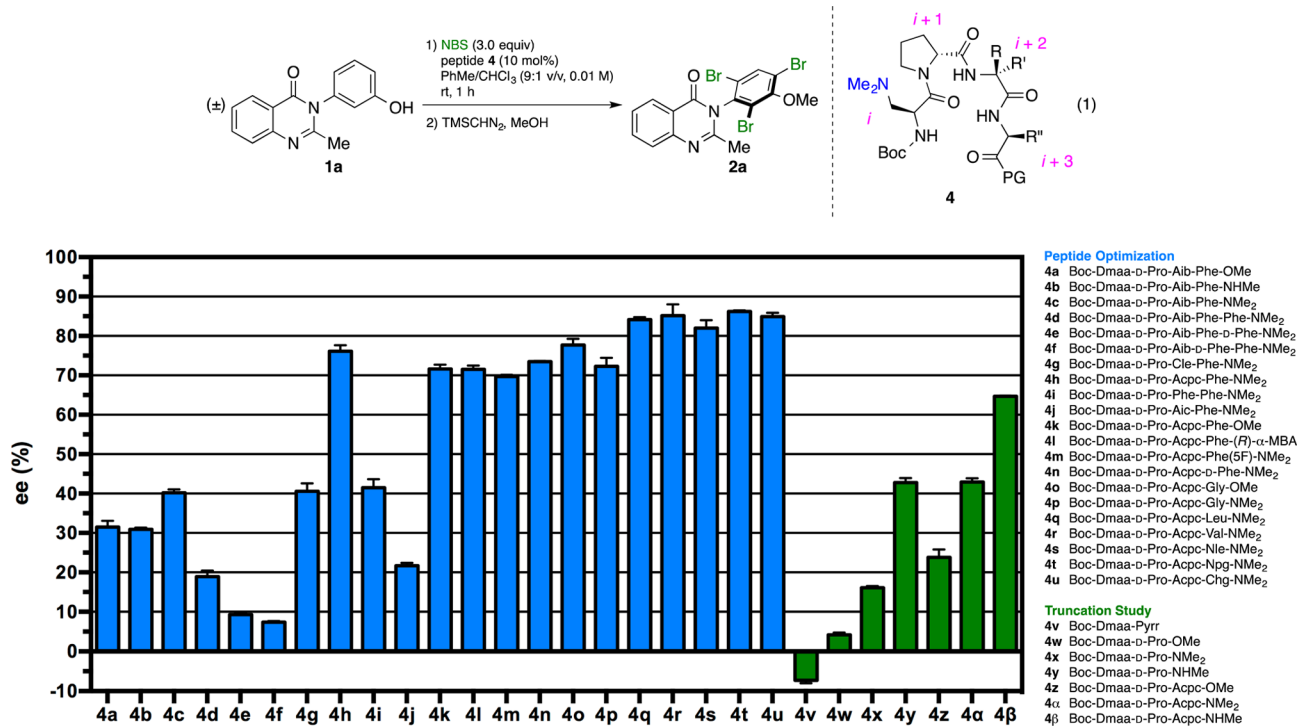


**Figure 2.** Assessment of peptide-based catalysts in the bromination of quinazolinone **1a** using the conditions described in eq 1. Data shown in blue are the results of peptide optimization studies, and data shown in green are the results of a truncation study. All results represent the average of two trials. Abbreviations: Boc, *tert*-butylcarbamate; Dmaa,  $\beta$ -dimethylaminoalanine; Aib, 2-aminoisobutyric acid; Cle, cycloleucine (1-aminocyclopentane carboxylic acid); Acpc, 1-aminocyclopropane carboxylic acid; Aic, 2-aminoindane carboxylic acid; (*R*)- $\alpha$ -MBA, (*R*)- $\alpha$ -methyl benzyl amide; Phe(*SF*), pentafluorophenylalanine; Nle, norleucine (*n*-butylglycine); Npg, neopentylglycine; Chg, cyclohexylglycine; Pyrr, pyrrolidinyl.

alternatives, which may be attributed to the enhanced hydrogen-bond acceptor ability of tertiary amides.<sup>20</sup>

The enantioselectivity of peptide-catalyzed reactions is often highly sensitive to residue substitutions, especially those at the *i*+2 residue,<sup>16</sup> a position that plays an important role in determining the secondary structural attributes of the peptide.<sup>21</sup> Upon examining the *i*+2 residue (as in **4c** and **4g–j**), we observed a pronounced increase in enantioselectivity when 1-aminocyclopropane carboxylic acid (Acpc) was substituted in this position (as in **4h**), providing **2a** in 88:12 er, an increase in 36% ee compared to **4c**. The origin of this remarkable effect is not fully understood, although we have hypothesized that changes in the  $\phi$  and  $\psi$  angles of the  $\beta$ -turn conformation manifest in a more favorable interaction with **1a**.<sup>16,21</sup> A steric effect is also possible, although the degree of enhancement associated with the cyclopropyl ring of **4h** relative to the corresponding *gem*-dimethyl moiety of peptide **4c** may be too pronounced to be explained by sterics alone. Nonetheless, having found a suitable *i*+2 residue, we elected to re-examine the C-terminal protecting group to ensure that the trends upheld with Acpc at the *i*+2 position (as in **4h** and **4k,l**). Indeed, the dimethylamide C-terminal cap (as in **4h**) was again found to outperform the other functionalities.

Alterations to the *i*+3 position of  $\beta$ -turn-containing tetramers allowed for fine-tuning of enantioselectivity. Comparing peptides **4h** and **4m–u**, a number of trends emerged. First, it is clear that none of these changes produced as dramatic an effect as substitutions to the *i*+2 residue. Yet, it was also apparent that alkyl-substituted residues (**4q–u**) provide higher enantioenrichment of **2a** than benzyl-substituted (**4h**, **4m,n**) and unsubstituted (**4o,p**) residues. There was also very little difference among the alkyl-substituted *i*+3 residues of peptides **4q–u**, so we opted to move forward using leucine-containing **4q** as the lead catalyst, which provided tribromide **2a** in 92:8 er under the conditions of eq 1. Compared to peptide **4t**, which contained a slightly bulkier neopentylglycine (Npg) residue at the *i*+3 position and provided **2a** in 93:7 er, peptide **4q** had the added benefit of containing a proteinogenic, inexpensive, and readily available residue at the *i*+3 position.

**Catalyst Structure.** Catalyst **4q** proved amenable to study with X-ray diffraction (Figure 3). Interestingly, two different

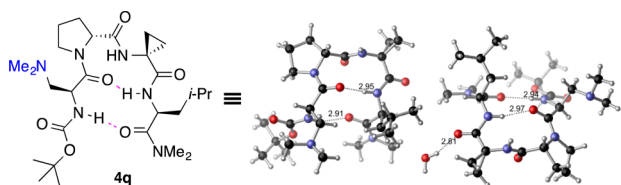


**Figure 3.** X-ray crystal structure of Boc-Dmaa-D-Pro-Acpc-Leu-NMe<sub>2</sub> (**4q**).<sup>24</sup> Two different conformations of **4q** are present in the unit cell, both of which show intramolecular hydrogen bonds characteristic of type II'  $\beta$ -turns.<sup>21</sup>

conformations of **4q** are present in the unit cell, one of which has an extended backbone (as drawn) while the other exhibits a backbone bend of nearly 110° out-of-plane. We have observed this sort of backbone bending previously,<sup>22</sup> although it remains unclear if this geometry is representative of active catalytic species. Nonetheless, both structures exhibit intramolecular hydrogen-bonding patterns and  $\phi$  and  $\psi$  dihedral angles consistent with a type II'  $\beta$ -turn.<sup>21</sup> We also studied the structure of **4q** in solution using <sup>1</sup>H–<sup>1</sup>H NOESY, and we were able to

observe 50 nonsequential nuclear Overhauser effects (NOEs) consistent with a rigid  $\beta$ -turn geometry (see Supporting Information).

Furthermore, we were able to demonstrate the importance of the folded conformation of peptide **4q** through a study of truncated peptide catalysts (Figure 2). The effect of sequential residue deletions on the outcome of the bromination reaction was dramatic. For example, we found that the trimer Boc-Dmaa-D-Pro-Acpc-NHMe (**4 $\beta$** ), which is able to access the intramolecular, 10-membered-ring hydrogen bond (NH<sub>*i*+3</sub> to O<sub>*i*</sub>) required for  $\beta$ -turn formation,<sup>21</sup> provided **2a** in 82:18 er, only modestly reduced compared to tetramer **4q**. On the other hand, trimers possessing methyl ester (**4z**) and dimethylamide (**4 $\alpha$** ) end-caps, which cannot form the  $\beta$ -turn hydrogen bond, were significantly less selective. This provides evidence that the  $\beta$ -turn secondary structure, which is accessible in tetramers and secondary amide-terminated trimers, is important for high levels of enantioinduction. Dimers **4w,x** were significantly less selective than the corresponding trimers, although we were intrigued to discover that one dimer, Boc-Dmaa-D-Pro-NHMe (**4y**), was equally selective to trimer **4 $\alpha$** , delivering **2a** in 72:28 er. It is possible that the enhanced selectivity exhibited by dimer **4y** derives from its ability to form a seven-membered-ring hydrogen-bonded structure (NH<sub>*i*+2</sub> to O<sub>*i*</sub>),<sup>23</sup> reinforcing the importance of secondary structure to enantioselectivity. It is also interesting to note that the inherent selectivity of the Dmaa monomer (**4v**) actually favors the opposite enantiomer of **2a**, albeit with very low er.

**Optimization of Reaction Conditions.** Having identified catalyst **4q** that is able to deliver tribromide **2a** in 92:8 er under the conditions of eq 1, in which *N*-bromosuccinimide (NBS) was added in one portion at the outset of the reaction, we wondered if we might be able to boost the enantioselectivity by changing the mode of NBS delivery. This speculation was borne of the hypothesis that full and rapid racemization of the starting material is required in order to achieve the best possible results in a dynamic kinetic resolution.<sup>3</sup> 2-Substituted 3-arylquinazolones, such as **1a**, have been reported to have intrinsic barriers to rotation about the N–C<sub>Ar</sub> bond, even in the absence of *ortho*-substituents on the phenol ring, that could impede rapid racemization as a dynamic kinetic resolution proceeds.<sup>13</sup> Therefore, we speculated that, if the barrier to enantiomerization<sup>27</sup> of **1a** is sufficiently high, the starting material may not be able to re-racemize on the time scale of a very rapid and stereodetermining bromination event. Indeed, density functional theory (DFT) calculations<sup>25</sup> showed that the barrier to enantiomerization in **1a** is 18.8 kcal mol<sup>−1</sup>, corresponding to a first-order half-life of 6.9 s (Figure 4), which may be slow with

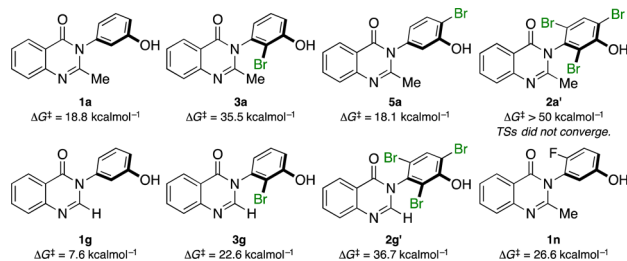
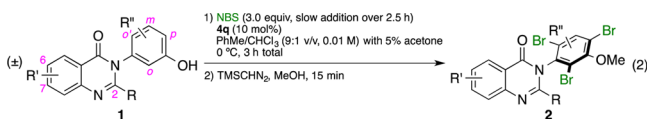


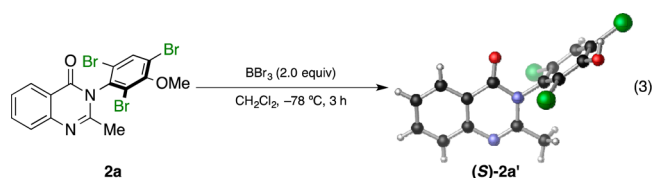
**Figure 4.** Computed barriers to rotation about the N–C<sub>Ar</sub> bond in a series of relevant quinazolones. Barriers were derived from optimization of the stationary points along torsional potential energy profiles using M06-2X/6-311++G(2d,3p)//B3LYP/6-31+G(d,p).<sup>25,26</sup>

respect to the time scale of bromination. After optimization of the relevant parameters, we discovered that slow addition of NBS over 2.5 h at 0 °C, as described in eq 2 (R = Me), provided **2a** in a



notably improved 97:3 er.<sup>28</sup> It is important to note that this increase in selectivity was observed even in the presence of 5% (by volume) acetone,<sup>10a</sup> which was added to the delivery solution to facilitate dissolution of the NBS.

**Substrate Scope.** With optimal conditions in hand, we turned our attention to the substrate scope. Catalyst **4q** is able to address a wide range of quinazolinones **1** (Table 1). As noted, the bromination of **1a** affords tribromide **2a** with 97:3 er and 86% isolated yield (entry 1). In order to establish the absolute configuration of the product, we subjected **2a** to standard demethylation conditions using BBr<sub>3</sub> to obtain free phenol **2a'**,<sup>29</sup> which we were able to crystallize and analyze by X-ray diffraction (eq 3). The crystal structure of **2a'** reveals the (*S*)-absolute stereochemistry of **2a**.



Quinazolinones possessing alkyl substituents at the 2-position (**1b–e**) were processed by **4q** with good yields (75–86%) and high levels of enantioinduction (93:7 to 97:3 er, entries 2–5). However, 2-CF<sub>3</sub>-substituted **1f** did not follow this same trend, as bromination delivered only 63% yield of modestly enriched **2f** (63:37 er, entry 6). The result was initially surprising given the high levels of enantioselectivity observed in tribromide **2c** (96:4 er, entry 3), as the steric size of a CF<sub>3</sub> group is comparable to an *i*-Pr group on some scales.<sup>30</sup> It appears that the electron-withdrawing CF<sub>3</sub> group of **1f** influences the catalyst–substrate complex in a manner we do not fully understand. Yet, we also observed low levels of enantioenrichment in tribromide **2g** (65:35 er, entry 7), in which the 2-position is unsubstituted. The origin of this phenomenon may derive from a low barrier to rotation about the chiral axis in the corresponding *ortho*-

Table 1. Substrate Scope<sup>a,b</sup>

Entry	Quinazolinone	Product	Yield <sup>c</sup>	e.r. <sup>d</sup>
1			86%	97:3
2			79%	97:3
3			78%	96:4
4			79%	96:4
5			75%	93:7
6			63%	63:37
7			80%	65:35
8			85%	95:5
9			85%	93:7
10 <sup>e</sup>			93%	96:4
11 <sup>e</sup>			92%	99:1
12			89%	96:4
13			77%	98:2
14 <sup>e</sup>			84%	56:44

<sup>a</sup>Reaction conditions: quinazolinone **1** (0.10 mmol, 1 equiv), peptide **4q** (0.01 mmol, 10 mol % with respect to **1**), NBS (0.30 mmol, 3 equiv with respect to **1**), PhMe/CHCl<sub>3</sub> (9:1 v/v) with 5% acetone additive (by volume), slow addition of NBS over 2.5 h. <sup>b</sup>Data represent the average of two trials. <sup>c</sup>Isolated yields after chromatography are presented. <sup>d</sup>Enantiomer ratios were determined by chiral high-performance liquid chromatography using OJ-H or AD-H columns. <sup>e</sup>2.0 equiv of NBS were used in the bromination.



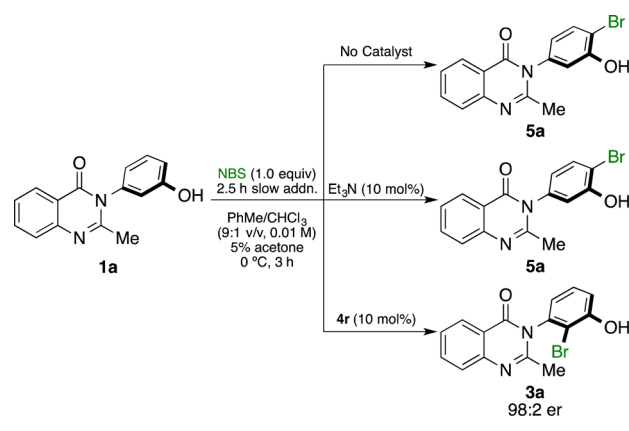
monobromide **3g**, which we presume is the immediate product of stereodetermining bromination. Indeed, using DFT calculations,<sup>25</sup> we were able to compute a barrier to rotation of 22.6 kcal mol<sup>-1</sup> in monobromide **3g**, which may be sufficiently low to permit racemization on the time scale of the slow addition. By way of comparison, the computed rotational barriers for quinazolinone **1g** and tribromide **2g'** were found to be 7.6 and 36.7 kcal mol<sup>-1</sup>, respectively, using DFT computations (Figure 4).<sup>25</sup>

Many other substrates were brominated by **4q** with high levels of enantioselectivity. For example, we found that substitution on the benzo moiety of the quinazolinone scaffold is often tolerated (entries 8 and 9). Tribromide **2h**, having an electron-donating methoxy group at the 6-position, was isolated in 85% yield and 95:5 er, only slightly lower than the parent compound (entry 8). Likewise, 7-CF<sub>3</sub>-substituted tribromide **2i** was isolated in 85% yield and 93:7 er (entry 9). These results suggest a weak effect of distal substitution on enantioselectivity, though both electron-donating and electron-withdrawing groups are still largely tolerated by **4q**. Substitution on the phenol moiety of the quinazolinone scaffold also revealed interesting data. The *p*-Cl-substituted dibromide **2j** was isolated in excellent yield (93%) and with 96:4 er (entry 10). We also found that tribromide **2l**, which was derived from the *m*-Cl-substituted quinazolinone **1l**, was isolated in high yield (89%) and with 96:4 er (entry 12). These results show that peptide **4q** is able to process substrates possessing electron-withdrawing substituents on the arene with negligible erosion of enantioselectivity relative to **2a**. In addition, electron-donating Me substituents at the *p*- (**1k**) and *m*-positions (**1m**) provide excellent substrates, as dibromide **2k** was isolated in 92% yield with 99:1 er (entry 11) and tribromide **2m** was isolated in 77% yield and 98:2 er (entry 13).<sup>31</sup>

Lastly, we examined a compound that was prefunctionalized at the *o'*-position of the phenol moiety. In this case, we anticipated a reduced er value by virtue of a high barrier to racemization in the starting material. Indeed, *o'*-F-substituted **1n** was found to deliver dibromide **2n** in only 56:44 er (entry 14). DFT calculations<sup>25</sup> showed that **1n** has a 26.6 kcal mol<sup>-1</sup> barrier to rotation about the chiral axis (Figure 4), corresponding to a half-life to rotation of 3.6 × 10<sup>6</sup> s. Thus, racemization is presumed to be slow on the time scale of bromination. In this scenario, compound **1n** was projected to be a suitable substrate for a traditional kinetic resolution.<sup>32</sup> Accordingly, running the bromination of **1n** to low conversion using only 0.5 equiv of NBS under otherwise identical conditions delivered **2n** in 93:7 er (14% isolated yield), showing that quinazolinones with high barriers to racemization may indeed be synthesized enantioselectively, employing a classical kinetic resolution.

**Mechanism-Driven Experiments.** Examination of the substrate scope inspired us to investigate certain mechanistic aspects of this enantioselective bromination reaction. We began with an LC/MS-enabled study of the background and catalyzed bromination of **1a** under conditions of reagent-controlled low conversion (Scheme 1). As noted above, in the absence of catalyst, the bromination proceeds slowly, and in fact, the major species in the crude reaction mixture is the *p*-monobromide **5a**, although all mono-, di-, and tribromides were observed in minor quantities. When triethylamine is used as a catalyst, the reaction proceeds more efficiently and with significant regioselectivity, also favoring the *p*-monobromide **5a** with no evidence of the other monobromides. The *o,p*-dibromide was also formed in approximately equal quantities under the triethylamine conditions, and the tribromide was observed as a minor product.

**Scheme 1. Study of the Major Monobromides in the Catalyzed and Uncatalyzed Bromination of 1a**



Using peptide **4r**, which provides enantioselectivity similar to that of **4q** (vide supra), the reaction constrained to reach low conversion exhibits a strikingly different result: the major monobromide is the alternative regioisomer **3a**, while only a very small quantity of the *p*-monobromide **5a** is detected, while the *o,p*-dibromide and tribromide **2a'** are also detected. These results indicate that the peptide-based catalyst is able to overturn the inherent site selectivity of the bromination reaction, which also implies that the stereodetermining bromination event is the first bromination to give **3a** (see Supporting Information for LC/MS data). Furthermore, when the crude reaction mixture of the **4r**-catalyzed reaction was subjected to methylation and analyzed by chiral high-performance liquid chromatography, it was discovered that monobromide **3a** was enantioenriched to 98:2 er. To the best of our knowledge, this is a rare example of an atroposelective reaction in which the chiral axis is set after the first functionalization of an atropisomerically dynamic starting material.<sup>33</sup>

To further our understanding of the basis of stereoselectivity, we studied the peptide–substrate complex using NMR techniques. The results of our findings are summarized in Figure 5. Compared to the <sup>1</sup>H NMR spectra of **1a** (Figure 5a) and **4q** (Figure 5c), the spectrum of the 1:1 complex (Figure 5b) differs significantly from its isolated constituents under identical conditions.<sup>34</sup> Notably, while the other amide signals shift downfield upon complexation, the NH<sub>Leu</sub> signal barely shifts at all, providing evidence for a strong hydrogen bond between NH<sub>Leu</sub> and O<sub>Dmaa</sub>. In contrast, the NH<sub>Acpc</sub> shifts downfield by nearly 1.0 ppm upon complexation, which implicates this proton in an important intermolecular hydrogen bond with **1a**. The NH<sub>Dmaa</sub> signal also shifts downfield by about 0.3 ppm, which may suggest a change in the β-hairpin conformation as a result of complexation. It may also implicate the carbamate NH proton in an interaction with the substrate.

Furthermore, we observed a global upfield shifting of all of the *i* + 3 leucine signals, especially the γ<sub>Leu</sub> signal. This suggests that the *i* + 3 residue might be situated beneath an arene, such that electron density in the π-system leads to this anisotropic effect. The α<sub>D-Pro</sub> signal also shifts upfield, presumably for similar reasons. Similarly, all of the Dmaa signals tend to shift downfield, in keeping with a decrease in electron density around the side-chain N-atom as would be expected in a Me<sub>2</sub>N<sub>Dmaa</sub> to HO<sub>1a</sub> hydrogen bond. It is also evident that the β<sub>Dmaa</sub> signals of **4q** become significantly more differentiated in the complex than in the free peptide. With respect to the substrate, all of the <sup>1</sup>H NMR

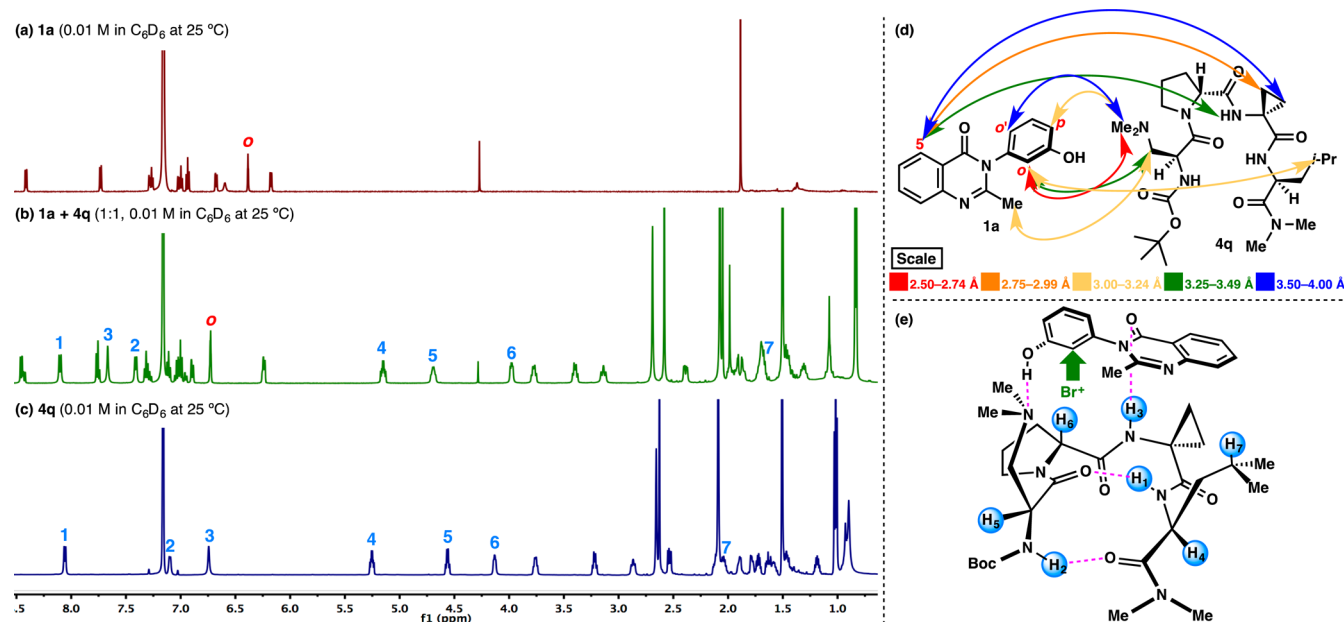


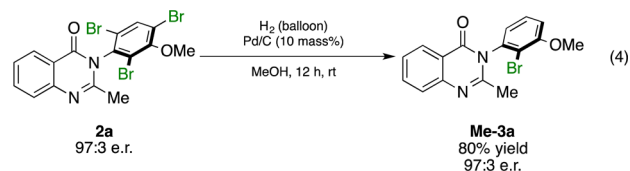
**Figure 5.** (a) <sup>1</sup>H NMR spectrum of quinazolinone **1a**. (b) <sup>1</sup>H NMR spectrum of the **1a**–**4q** complex (1:1 molar ratio). (c) <sup>1</sup>H NMR spectrum of peptide **4q**. (d) NOESY correlation diagram showing the intermolecular NOEs observed in the **1a**–**4q** complex. (e) Possible binding model based on NMR data. The model explains the (*S*)-absolute configuration of the products and also predicts the first site of bromination at the *ortho*-position of **1a**.

signals of **1a** shift downfield in the complex. However, only the *ortho*-position (Figure 5a) shifts downfield to a significant degree (>0.30 ppm), which may be consistent with this position being disposed most proximally to the peptide in the complex. In light of these results, as well as our mechanistic studies that identified this position as the site of the first bromination event, it seems plausible that the peptide delivers Br<sup>+</sup> to this position via one of the proximal Lewis basic carbonyls.<sup>35</sup> It should also be noted that many of the <sup>1</sup>H NMR signals corresponding to complexed **1a** possess minor shoulder peaks, while this is not evident in any of the signals derived from **4q**. This perhaps suggests that **1a** might be fluxional in the bound state. We also studied the binding interaction between **1a** and **4q** using <sup>1</sup>H–<sup>1</sup>H NOESY, and we were able to observe several intermolecular NOEs that supported this model. A summary of these interactions is presented in Figure 5d, where the color-coded distances are derived from integration of the relevant NOESY cross-peaks.<sup>36</sup> This experiment highlighted a number of interactions that were not observed in the simple <sup>1</sup>H NMR complexation experiment (vide supra). For instance, strong NOEs were observed between (1) Me<sub>2</sub>N<sub>D<sub>maa</sub></sub> and the *ortho*-position of **1a** and (2) β<sub>AcpC</sub> and the 5-position of **1a**, suggesting that these groups are very close to one another in space in the complex. Moderate NOEs were also observed between β<sub>D<sub>maa</sub></sub> and the 2-Me group of **1a**, as well as between the *i*-Pr group of leucine and the *ortho*-position of **1a**. Weak NOEs were also observed, allowing us to fine-tune our proposed binding orientation.

The culmination of these mechanistically driven studies is a self-consistent binding model from which we were able to rationalize the first site of bromination, as well as the (*S*)-absolute configuration of products **2** and *ortho*-monobromides **3** (Figure 5e). Our model suggests two intermolecular hydrogen bonds in the catalyst–substrate complex, one between OH<sub>1a</sub> and Me<sub>2</sub>N<sub>D<sub>maa</sub></sub> and the other between NH<sub>AcpC</sub> and C=O<sub>1a</sub>.

**Cross-Coupling.** With the atroposelective bromination of quinazolinones established, we turned to the demonstration of further synthetic utility through derivatization of the brominated

products.<sup>37</sup> Recognizing the prevalence of monosubstituted quinazolinones in the medicinal chemistry literature (Figure 1a),<sup>9</sup> we sought to establish that tribromide **2a** could be converted to **3a** efficiently and without loss of enantioenrichment. As shown in eq 4, palladium-catalyzed hydrogenation

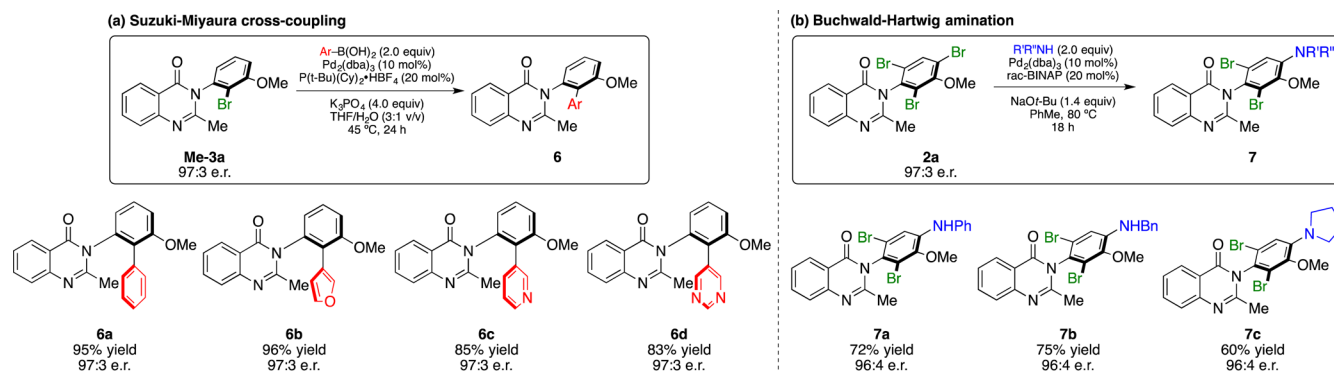


under well-established conditions achieved this goal,<sup>38</sup> affording monobrominated compound **Me-3a** in 80% yield with high levels of regioselectivity presumably governed by sterics. Despite the lack of a second heavy atom *ortho*'-substituent on the phenol ring, this compound exhibited good atropstability at ambient temperature. The barrier to rotation about the chiral axis in **3a** was calculated to be 35.5 kcal mol<sup>-1</sup> using DFT calculations,<sup>25</sup> which corresponds to a half-life of 1.13 × 10<sup>13</sup> s (Figure 4).

Monobromide **Me-3a** was then examined as a template for diversification. After initial studies of Suzuki–Miyaura cross-coupling<sup>39</sup> reactions revealed that some racemization could occur at high temperatures (>60 °C), we discovered that excellent results could be achieved at lower temperatures (45 °C) when a highly active catalyst was employed. Under the optimized conditions, Pd<sub>2</sub>(dba)<sub>3</sub> and (*t*-Bu)(Cy)<sub>2</sub>P·HBF<sub>4</sub> enabled the Suzuki coupling of **3a** with various arene and heterocycle boronic acids under atropstable conditions, providing good yields of structurally complex products (**6**) with no loss of enantioenrichment, as shown in Scheme 2a.

Upon the success of atropstable Suzuki coupling of **Me-3a**, we sought to expand the scope of our product derivatization beyond the formation of C–C bonds using Buchwald–Hartwig O- and N-arylation.<sup>40</sup> Unfortunately, under the conditions we had examined thus far, which required high temperatures of ~80 °C for product formation, products were observed with reduced

Scheme 2. Cross-Coupling of Quinazolinone Bromides



levels of enantioenrichment, suggesting racemization during the reaction.<sup>41</sup> However, the more atropisomerically stable tribromide **2a**, having a computed barrier to enantiomerization of over 50 kcal mol<sup>-1</sup> (**2a'**, Figure 4),<sup>42</sup> proved to be a good substrate, wherein regioselective amination could be achieved to form compounds such as **7a–c** in good yields and with very little erosion of er (Scheme 2b). The site selectivity of the amination is presumably due to steric differentiation.

## CONCLUSIONS

Peptide-catalyzed atroposelective bromination has been extended to a highly significant scaffold in medicinal chemistry. Critical to the achievement of this advance were the discovery of an optimized catalyst and an appreciation of the physical organic principles that govern the barriers to rotation in the starting materials and products for these unique reactions. Catalyst **4q** was found to be effective for a broad substrate scope, and moreover, the unique conformational properties (i.e., barriers to atropisomerization) of the products enable site-selective debromination and cross-coupling reactions of several types to deliver multiple drug-like chemotypes. Mechanism-driven experiments have also revealed a number of interesting features of these asymmetric reactions, including the likely site of the initial and stereodetermining bromination. NMR spectroscopic experiments have unveiled critical features of the catalyst–substrate complex that are consistent with the observation of the absolute configuration of the products that emerge from these reactions. It is our hope that these concepts set the stage for synthetic applications in the context of this biologically relevant scaffold.

## ASSOCIATED CONTENT

### Supporting Information

The Supporting Information is available free of charge on the ACS Publications website at DOI: 10.1021/jacs.5b07726.

Additional experimental details, characterization data for all catalysts, substrates, and products, crystallographic information, and computational data (PDF)

X-ray data of **4q** (CIF)

X-ray data of (*S*)-**2a'** (CIF)

## AUTHOR INFORMATION

### Corresponding Author

\*scott.miller@yale.edu

## Present Address

‡Department of Chemistry, Faculty of Science, Fukuoka University, Fukuoka 814–0180, Japan.

## Author Contributions

†M.E.D. and A.J.M. contributed equally to the project.

## Notes

The authors declare no competing financial interest.

Crystallographic data are deposited with the Cambridge Crystallographic Data Centre under the accession number CCDC 1412919 (**2a'**) and CCDC 1412920 (**4q**).

## ACKNOWLEDGMENTS

We are grateful to the National Institute of General Medical Sciences of the NIH (GM-068649) for support. A.J.M. would like to extend his sincerest thanks to the NSF Graduate Research Fellowship Program for financial support. We would like to thank Dr. Eric Paulson for his assistance with our NMR studies, and Dr. Brandon Mercado for solving our X-ray crystal structures. We would also like to thank Nadia Abascal, Dr. Guillaume Pelletier, and Dr. Byoungmoo Kim for helpful discussions. All computational work was supported by the facilities and staff of the Yale University Faculty of Arts and Sciences High Performance Computing Center and by the National Science Foundation under Grant No. CNS 08-21132 that partially funded acquisition of the facilities.

## REFERENCES

- (1) Ōki, M. Recent Advances in Atropisomerism. In *Topics in Stereochemistry*; Allinger, N. L., Eliel, E. L., Wilen, S. H., Eds.; Wiley: Hoboken, NJ, 1983; Vol. 14, pp 1–81.
- (2) For relevant reviews, please see: (a) LaPlante, S. R.; Fader, L. D.; Fandrick, K. R.; Fandrick, D. R.; Hucke, I.; Kemper, R.; Miller, S. P. F.; Edwards, P. J. *J. Med. Chem.* **2011**, *54*, 7005–7022. (b) LaPlante, S. R.; Edwards, P. J.; Fader, L. D.; Jakalian, A.; Hucke, O. *ChemMedChem* **2011**, *6*, 505–513. (c) Clayden, J.; Moran, W. J.; Edwards, O. J.; LaPlante, S. R. *Angew. Chem., Int. Ed.* **2009**, *48*, 6398–6401.
- (3) For reports on dynamic kinetic resolution, please see: (a) Pellissier, H. *Tetrahedron* **2011**, *67*, 3769–3802. (b) Pellissier, H. *Tetrahedron* **2008**, *64*, 1563–1601. (c) Faber, K. *Chem. - Eur. J.* **2001**, *7*, 5004–5010. (d) Ward, R. S. *Tetrahedron: Asymmetry* **1995**, *6*, 1475–1490.
- (4) For reports describing the differential, and perhaps deleterious, effects of drug enantiomers, please see: (a) Agranat, I.; Caner, H.; Caldwell, J. *Nat. Rev. Drug Discovery* **2002**, *1*, 753–768. (b) Shah, R. R.; Midgley, J. M.; Branch, S. K. *Adv. Drug. React. Toxicol. Rev.* **1998**, *17*, 145–190. (c) Reist, M.; Carrupt, P.-A.; Francotte, E.; Testa, B. *Chem. Res. Toxicol.* **1998**, *11*, 1521–1528. (d) Eriksson, T.; Bjorkman, S.; Roth, B.; Fyge, A.; Hoglund, P. *Chirality* **1995**, *7*, 44–52. (e) Fabro, S.; Smith,



R. L.; Williams, R. T. *Nature* **1967**, *215*, 296. (f) Ashrafiyan, H.; Horowitz, J. D.; Frenneaux, M. P. *Cardiovasc. Drug Rev.* **2007**, *25*, 76–97.

(5) For examples of differential biological function of individual drug atropisomers, please see: (a) LaPlante, S. R.; Forgione, P.; Boucher, C.; Coulombe, R.; Gillard, J.; Hucke, O.; Jakalian, A.; Joly, M.-A.; Kukolj, G.; Lemke, C.; McCollum, R.; Titolo, S.; Beaulieu, P. L.; Stammers, T. J. *Med. Chem.* **2014**, *57*, 1944–1951. (b) Eveleigh, P.; Hulme, E. C.; Schudt, C.; Birdsall, N. J. M. *Mol. Pharmacol.* **1989**, *35*, 477–483.

(6) Evarts, J. B.; Ulrich, R. G. Atropisomers of 2-puriny-3-arylquinazolinone derivatives and methods of use. U.S. Patent Appl. US 8,440,677 B2, 2013; Gilead Galistoga LLC, USA.

(7) For reviews on atroposelective synthesis, please see: (a) Bencivenni, G. *Synlett* **2015**, *26*, 1915–1922. (b) Wencel-Delord, J.; Panossian, A.; Leroux, F. R.; Colobert, F. *Chem. Soc. Rev.* **2015**, *44*, 3418–3430. (c) Bringmann, G.; Mortimer, A. J. P.; Keller, P. A.; Gresser, M. J.; Garner, J.; Breuning, M. *Angew. Chem., Int. Ed.* **2005**, *44*, 5384–5427.

(8) From this point forward, we will refer to 3-arylquinazolin-4(3H)-ones (**1**) as quinazolinones for simplicity.

(9) CP-465022: (a) Lazzaro, J. T.; Paternain, A. V.; Lerma, J.; Chenard, B. L.; Ewing, F. E.; Huang, J.; Welch, W. M.; Ganong, A. H.; Menniti, F. S. *Neuropharmacology* **2002**, *42*, 143–153. Benzomalivin A: (b) Sun, H. H.; Barrow, C. J.; Sedlock, D. M.; Gillum, A. M.; Cooper, R. J. *Antibiot.* **1994**, *47*, 515–522. (c) Sun, H. H.; Barrow, C. J.; Cooper, R. J. *Nat. Prod.* **1995**, *58*, 1575–1580. Erastin: (d) Gangadhar, N. M.; Stockwell, B. R. *Curr. Opin. Chem. Biol.* **2007**, *11*, 83–87. (e) Yagoda, N.; von Rechenberg, M.; Zaganjor, E.; Bauer, A. J.; Yang, W. S.; Fridman, D. J.; Wolpaw, A. J.; Smukste, I.; Peltier, J. M.; Boniface, J. J.; Smith, R.; Lessnick, S. L.; Sahasrabudhe, S.; Stockwell, B. R. *Nature* **2007**, *447*, 864–868.

(10) (a) Gustafson, J. L.; Lim, D.; Miller, S. J. *Science* **2010**, *328*, 1251–1255. (b) Garand, E.; Kamrath, M. Z.; Jordan, P. A.; Wolk, A. B.; Leavitt, C. M.; McCoy, A. B.; Miller, S. J.; Johnson, M. A. *Science* **2012**, *335*, 694–698.

(11) (a) Barrett, K. T.; Miller, S. J. *J. Am. Chem. Soc.* **2013**, *135*, 2963–2966. (b) Barrett, K. T.; Metrano, A. J.; Rablen, P. R.; Miller, S. J. *Nature* **2014**, *509*, 71–75.

(12) Miyaji, R.; Asano, K.; Matsubara, S. *J. Am. Chem. Soc.* **2015**, *137*, 6766–6769.

(13) For examples of methods providing access to enantioenriched 3-arylquinazolin-4(3H)-ones, please see: (a) Tokitoh, T.; Kobayashi, T.; Nakada, E.; Inoue, T.; Yokoshima, S.; Takahashi, H.; Natsugari, H. *Heterocycles* **2006**, *70*, 93–99. (b) Penhoat, M.; Bohn, P.; Dupas, G.; Papamicaël, C.; Marsais, F.; Levacher, V. *Tetrahedron: Asymmetry* **2006**, *17*, 281–286. (c) Dai, X.; Wong, A.; Virgil, S. C. *J. Org. Chem.* **1998**, *63*, 2597–2600.

(14) (a) Azanli, E.; Rothchild, R.; Sapse, A.-M. *Spectrosc. Lett.* **2002**, *35*, 257–274. (b) Colebrook, L. D.; Giles, H. G. *Can. J. Chem.* **1975**, *53*, 3431–3434. (c) Mannschreck, A.; Kaller, H.; Stühler, G.; Davies, M. A.; Traber, J. *Eur. J. Med. Chem. Chim. Ther.* **1984**, *19*, 381.

(15) The reaction solvent was rigorously optimized in the early stages of this project. We found that 9:1 v/v PhMe/CHCl<sub>3</sub> delivered higher enantioselectivities than pure PhMe, pure CHCl<sub>3</sub>, 9:1 v/v CHCl<sub>3</sub>/PhMe, and 9:1 v/v CHCl<sub>3</sub>/C<sub>6</sub>F<sub>6</sub>. Furthermore, the concentration of the reaction (0.01 M) was also optimized at an early stage. Dilution beyond 0.01 M served to decrease yield with no effect on enantioselectivity. Concentrations greater than 0.01 M provided lower er values, presumably due to an acceleration of the background rate.

(16) For relevant reviews, see: (a) Miller, S. J. *Acc. Chem. Res.* **2004**, *37*, 601–610. (b) Jarvo, E. R.; Miller, S. J. *Tetrahedron* **2002**, *58*, 2481–2495. For recent examples of  $\beta$ -turn peptides in enantioselective reactions, see: (c) Metrano, A. J.; Miller, S. J. *J. Org. Chem.* **2014**, *79*, 1542–1554. (d) Mbofana, C. T.; Miller, S. J. *J. Am. Chem. Soc.* **2014**, *136*, 3285–3292. (e) Romney, D. K.; Miller, S. J. *Org. Lett.* **2012**, *14*, 1138–1141. (f) Peris, G.; Jakobsche, C. E.; Miller, S. J. *J. Am. Chem. Soc.* **2007**, *129*, 8710–8711.

(17) The bromination of **1a** in the absence of catalysts provides <5% yield of tribromide **2a**. The majority of **1a** is converted to a complex mixture of monobromides and dibromides, with the monobromides being favored. Please consult the [Mechanism-Driven Experiments](#)

section and the [Supporting Information](#) for more details. Dissolution of the starting materials is also poor when no catalyst is present.

(18) Only enantioselectivities were measured in the peptide optimization studies summarized in [Figure 2](#). Isolated yields were not assessed on small scale. Conversion of **1a** was always near quantitative by crude <sup>1</sup>H NMR.

(19) For examples of peptides taking advantage of a D-Pro-Aib  $\beta$ -turn sequence, see: (a) Fowler, B. S.; Mikochik, P. J.; Miller, S. J. *J. Am. Chem. Soc.* **2010**, *132*, 2870–2871. (b) Cowen, B. J.; Saunders, L. B.; Miller, S. J. *J. Am. Chem. Soc.* **2009**, *131*, 6105–6107. See also ref [11](#).

(20) Gilli, P.; Pretto, L.; Bertolasi, V.; Gilli, G. *Acc. Chem. Res.* **2009**, *42*, 33–44.

(21) (a) Haque, T. S.; Little, J. C.; Gellman, S. H. *J. Am. Chem. Soc.* **1996**, *118*, 6975–6985. (b) Wilmot, C. M.; Thornton, J. M. *J. Mol. Biol.* **1988**, *203*, 221–232.

(22) Blank, J. T.; Miller, S. J. *Biopolymers* **2006**, *84*, 38–47.

(23) (a) Gellman, S. H.; Dado, G. P.; Liang, G.-B.; Adams, B. R. *J. Am. Chem. Soc.* **1991**, *113*, 1164–1173. (b) Yang, D.; Zhang, D.-W.; Hao, Y.; Wu, Y.-D.; Luo, S.-W.; Zhu, N.-Y. *Angew. Chem.* **2004**, *116*, 6887–6890. (c) Trabocchi, A.; Potenza, D.; Guarna, A. *Eur. J. Org. Chem.* **2004**, *2004*, 4621–4627.

(24) CYLview was used to render the X-ray crystal data: CYLview, 1.0b; Legault, C. Y. Université de Sherbrooke, 2009 (<http://www.cylview.org>).

(25) DFT computations were performed using the Gaussian 09 suite: (a) Frisch, M. J.; Trucks, G. W.; Schlegel, H. B.; Scuseria, G. E.; Robb, M. A.; Cheeseman, J. R.; Scalmani, G.; Barone, V.; Mennucci, B.; Petersson, G. A.; Nakatsuji, H.; Caricato, M.; Li, X.; Hratchian, H. P.; Izmaylov, A. F.; Bloino, J.; Zheng, G.; Sonnenberg, J. L.; Hada, M.; Ehara, M.; Toyota, K.; Fukuda, R.; Hasegawa, J.; Ishida, M.; Nakajima, T.; Honda, Y.; Kitao, O.; Nakai, H.; Vreven, T.; Montgomery, J. A., Jr.; Peralta, J. E.; Ogliaro, F.; Bearpark, M.; Heyd, J. J.; Brothers, E.; Kudin, K. N.; Staroverov, V. N.; Kobayashi, R.; Normand, J.; Raghavachari, K.; Rendell, A.; Burant, J. C.; Iyengar, S. S.; Tomasi, J.; Cossi, M.; Rega, N.; Millam, J. M.; Klene, M.; Knox, J. E.; Cross, J. B.; Bakken, V.; Adamo, C.; Jaramillo, J.; Gomperts, R.; Stratmann, R. E.; Yazyev, O.; Austin, A. J.; Cammi, R.; Pomelli, C.; Ochterski, J. W.; Martin, R. L.; Morokuma, K.; Zakrzewski, V. G.; Voth, G. A.; Salvador, P.; Dannenberg, J. J.; Dapprich, S.; Daniels, A. D.; Farkas, Ö.; Foresman, J. B.; Ortiz, J. V.; Cioslowski, J.; Fox, D. J. *Gaussian 09*, Revision C.01; Gaussian, Inc.: Wallingford, CT, 2009. (b) In general, rotational barriers were derived from optimization of the stationary points of a relaxed torsional potential energy scan of the N–C<sub>Ar</sub> amide axis at the M06-2X/6-311++G(2d,3p)//B3LYP/6-31+G(d,p) level.<sup>26</sup> Frequency calculations were performed at the B3LYP/6-31+G(d,p) level, and all transition states were found to have one, single imaginary frequency corresponding to a vibration along the N–C<sub>Ar</sub> torsional reaction coordinate.

(26) Zhao, Y.; Truhlar, D. G. *Theor. Chem. Acc.* **2008**, *120*, 215–241. See also ref [11b](#).

(27) Reist, M.; Testa, B.; Carrupt, P.-A.; Jung, M.; Schurig, V. *Chirality* **1995**, *7*, 396–400.

(28) Slow addition was accomplished using a syringe pump. We found that using an 18 gauge needle avoided clogging via NBS precipitation over the 2.5 h slow addition. The rate of addition (1.60 mL min<sup>-1</sup>), length of addition (2.5 h), and composition/volumes of delivery (3.5 mL of 9:1 v/v PhMe/CHCl<sub>3</sub> with 0.5 mL of acetone additive, 4 mL total) and source (6 mL of 9:1 v/v PhMe/CHCl<sub>3</sub>) solutions were rigorously optimized for the 0.10 mmol scale reaction. Additional details on the optimization of the reaction conditions may be found in the [Supporting Information](#).

(29) (a) McOmie, J. F. W.; Watts, M. L.; West, D. E. *Tetrahedron* **1968**, *24*, 2289–2292. (b) This reaction was performed on small scale, and isolated yield was not obtained following crystallization.

(30) Hirsch, J. A. Table of Conformational Energies. In *Topics in Stereochemistry*; Allinger, N. L., Eliel, E. L., Eds.; Wiley: Hoboken, NJ, 1967; Vol. 1, pp 199–222.

(31) In the case of **2k**, we hypothesized that the marked increase in enantioselectivity to 99:1 er (relative to 97:3 er in **2a**, corresponding to  $\Delta\Delta G^\ddagger = 0.61$  kcal mol<sup>-1</sup> at 0 °C) may be due to (1) the Me group being



electron-releasing and thereby ring-activating and (2) the Me group blocking the position of the first bromination in the uncatalyzed background reaction (see [Mechanism-Driven Experiments](#) section). In that way, the catalyzed reaction outcompetes the background reaction significantly. In the case of **2m**, ring activation of the *meta*-Me-substituent provides an increase to 98:2 er relative to the parent, but the background pathway is still possible via bromination at the *para*-position. The results obtained for Cl-substituted **2j** and **2l** (both 96:4 er) might suggest that ring activation is important to the er of the reaction. Steric effects may also be at play in these instances.

(32) (a) Keith, J. M.; Larrow, J. F.; Jacobsen, E. N. *Adv. Synth. Catal.* **2001**, *343*, 5–26. (b) Kagan, H. B.; Fiaud, J. C. Kinetic Resolution. In *Topics in Stereochemistry*; Eliel, E. L., Wilen, S. H., Eds.; Wiley: Hoboken, NJ, 1988; Vol. 18, pp 249–340.

(33) Based purely on rotational barriers, many previously studied systems, including biaryls and benzamides, require two functionalization events (one at each *ortho*-position) to lock the asymmetric axis. See refs [10](#) and [11](#).

(34) The NMR studies were performed in C<sub>6</sub>D<sub>6</sub> to simulate the bulk PhMe of the reaction conditions (eq 2) without having two residual solvent lines in the spectrum. Even though the catalytic reaction is run at 0.001 M with respect to peptide **4q**, we opted to perform our NMR studies at 0.01 M to obtain better signal-to-noise. We verified that **4q** does not aggregate at 0.01 M solution by comparing <sup>1</sup>H NMR spectra of **4q** at 0.001 and 0.01 M under otherwise identical conditions. No change was observed in the proton signals at the higher concentration relative to the more dilute sample.

(35) For a related example, please see: Denmark, S. E.; Burk, M. T. *Proc. Natl. Acad. Sci. U. S. A.* **2010**, *107*, 20655–20660.

(36) (a) Cavanagh, J.; Fairbrother, W. J.; Palmer, A. G.; Rance, M.; Skelton, N. G. *Protein NMR Spectroscopy: Principles and Practice*, 3rd ed.; Elsevier Academic Press: Boston, MA, 2007. (b) Abascal, N. C.; Lichtor, P. A.; Giuliano, M. W.; Miller, S. J. *Chem. Sci.* **2014**, *5*, 4504–4511. (c) Lichtor, P. A.; Miller, S. J. *J. Am. Chem. Soc.* **2014**, *136*, 5301–5308.

(37) For related examples, please see: (a) Barrett, K. T.; Miller, S. J. *Org. Lett.* **2015**, *17*, 580–583. (b) Gustafson, J. L.; Lim, D.; Barrett, K. T.; Miller, S. J. *Angew. Chem., Int. Ed.* **2011**, *50*, 5125–5129.

(38) For an example of reductive dehalogenation of aryl bromides using Pd/C, please see: (a) Ramanathan, A.; Jimenez, L. S. *Synthesis* **2010**, *2010*, 217–220. For an example of a regioselective dehalogenation of aryl bromides, please see: (b) Chae, J.; Buchwald, S. L. *J. Org. Chem.* **2004**, *69*, 3336–3339.

(39) For examples of Suzuki–Miyaura cross-coupling of aryl halides in the context of quinazolinone scaffolds, please see: (a) Garlapati, R.; Pottabathini, N.; Gurram, V.; Kasani, K. S.; Gundla, R.; Thulluri, C.; Machiraju, P. K.; Chaudhary, A. B.; Addepally, U.; Dayam, R.; Chunduri, V. R.; Patro, B. *Org. Biomol. Chem.* **2013**, *11*, 4778–4791. (b) Fang, X.; Chen, Y. T.; Sessions, E. H.; Chowdhury, S.; Vojkovsky, T.; Yin, Y.; Pocas, J. R.; Grant, W.; Schröter, T.; Lin, L.; Ruiz, C.; Cameron, M. D.; LoGrasso, P.; Bannister, T. D.; Feng, Y. *Bioorg. Med. Chem. Lett.* **2011**, *21*, 1844–1848. (c) Li, H.-y.; Wang, Y.; McMillen, W. T.; Chatterjee, A.; Toth, J. E.; Mundla, S. R.; Voss, M.; Boyer, R. D.; Sawyer, J. S. *Tetrahedron* **2007**, *63*, 11763–11770.

(40) For examples of Buchwald–Hartwig amination reactions of aryl bromides, please see: (a) Driver, M. S.; Hartwig, J. F. *J. Am. Chem. Soc.* **1996**, *118*, 7217–7218. (b) Wolfe, J. P.; Wagaw, S.; Buchwald, S. L. *J. Am. Chem. Soc.* **1996**, *118*, 7215–7216.

(41) The computed half-life to enantiomerization in monobromide **3a** is 27 years at 80 °C,<sup>25</sup> which perhaps suggests that the species that undergoes racemization under the attempted cross-coupling conditions is not monobromide **Me-3a**. It is possible that the aryl-palladium species formed upon oxidative addition has a lower barrier to enantiomerization by way of a significantly lengthened bond.

(42) The transition states to enantiomerization of **2a'** were never found explicitly using the computational methods described in ref [25](#). The reported barrier of >50 kcalmol<sup>-1</sup> is derived from the torsional scan computation (see [Supporting Information](#) for details).